OTFS vs. OFDM in High-Speed Vehicular Traffic Scenarios

OTFS vs. OFDM in High-speed Vehicular Traffic Scenarios

Alessandro Compagnoni
Politecnico di Torino
Torino, Italy

Riccardo Tuninato
Politecnico di Torino
Torino, Italy

Carla Fabiana Chiasserini
Politecnico di Torino
Torino, Italy

Roberto Garello
Politecnico di Torino
Torino, Italy

Alessandro Nordio
CNR-IEIIT
Torino, Italy

Emanuele Viterbo
Monash University
Melbourne, Australia

***Abstract*—The growing interest in Orthogonal Time Frequency Space (OTFS) modulation for vehicular communication systems requires the validation of its advantages using suitable channel models capable of emulating the dynamic and geometric complexities of vehicle-to-infrastructure systems. This paper presents a novel, realistic geometric-based channel model, called V-CORE, specifically designed for evaluating the performance of OTFS in vehicular scenarios. Our model accurately characterizes the scattered paths by exploiting the radar cross-section of the vehicles that populate a road according to a given vehicular traffic intensity. Multiple road scenarios with different geometry and vehicle velocities are considered, resulting in a flexible tool to evaluate system performance in different traffic contexts. The V-CORE model provides the channel variables, particularly relevant to OTFS implementation, such as multipath Doppler shift, and delay. We assess the performance of OTFS against that of OFDM under different road structures, traffic intensity, and vehicle velocities. Further, we compare the proposed V-CORE model to the Extended Vehicular A model and demonstrate that ours provides a deeper insight into performance in high-speed vehicular scenarios.**

***Index Terms*—OTFS, 5G/6G, Connected vehicles, Channel modeling, Mobility**

I. Introduction

The 5G mobile standard, as its predecessor LTE, has adopted Orthogonal Frequency-Division Multiplexing (OFDM) modulation, given its good performance and robustness against multipath fading. Nevertheless, OFDM-based systems may still exhibit significant inter-carrier interference in the presence of mobile devices, as the Doppler shift affecting the signal and its scattered replicas can disrupt subcarriers' orthogonality [1]. Orthogonal Time Frequency Space (OTFS) modulation has thus emerged as an attractive alternative when Doppler shift is of primary concern [2]. The key idea of this new modulation scheme is to represent the wireless channel in the delay-Doppler domain, to get a more compact and sparse representation of the parameters. OTFS is then of high interest for high-mobility communication scenarios such as vehicular networks, which are gaining momentum as connected autonomous driving is one of the target applications of 5G and 6G systems.

Vehicular scenarios require channel models that can accurately capture the behavior of communication links when at least one end-point is a highly mobile node. Notably, the 3GPP standard [3] includes different multipath fading channels suitable for low, medium, and high delay spread environments, where the medium one represents the Extended Vehicular A model (EVA), specifically designed for vehicular systems in urban and suburban areas [4]. EVA defines 9 distinct channel taps, with fixed delays and average power. Typically, each path uses a Jakes Doppler spectrum. This stochastic channel model is widely used in simulations but fails to provide insights into system performance for different vehicular scenario settings. Other approaches [5] instead, generate the channel via sophisticated ray-tracing methods that can accurately characterize the signal propagation in a given environment. Such models are very effective but highly complex and often too specific for evaluating the system performance in other scenarios of interest. A convenient trade-off between stochastic and ray-tracing channel models is represented by the Geometric-based stochastic channel models (GBSCMs) where reflectors are positioned according to a probability distribution and the resulting received signal is determined by the sum of the ray-tracing solutions of each signal reflector component. For instance, in [6] reflectors are uniformly distributed within a circle around the mobile terminal, aiming to model a fading channel in a macrocellular mobile environment. Reference [7], instead, presents a geometrical channel model characterizing vehicle-to-vehicle MIMO-based communication, while [8] leverages on the theory of ambit processes for fast simulations and spatial consistency of multipath.

Several works have addressed the relationship between the wireless channel behavior and OTFS performance. In particular, [9] proposes a linear complexity iterative rake detector for OTFS, and compares its performance to OFDM under EVA channel. A new detection and channel estimation scheme is introduced in [10], adopting a high-Doppler synthetic fading channel. The study in [11] adopts the latest 3GPP Tapped Delay Line (TDL) channel model for evaluating the OTFS bit error rate (BER) and includes an extension for fast fading with Doppler shift, while [12] compares OTFS and OFDM in a mobility scenario for two different dynamic 3D vehicles, under the Ray-launching model. Finally, [13] characterizes the vehicular channel leveraging mmWave vehicular crossroads

measurements, to assess sparsity in the delay-Doppler domain.

A. Our Contribution

Previous works have evaluated OTFS, but using generic channel models, such as EVA, or under very specific conditions obtained through channel measurements in certain given areas. Our goal is instead to design a channel model that (i) accurately represents the multipath propagation given by the surrounding vehicles, and (ii) is flexible and capable of modeling different traffic conditions and road geometries. We thus opt for a geometric-based stochastic channel model (GBSCM) approach and develop a model, named Vehicular Communication with Reflectors (V-CORE) model, that can relate the wireless channel variables with the actual elements of a vehicle-to-infrastructure (V2I) communication environment. In particular, V-CORE well models highway and country road scenarios, where signal reflections are mostly caused by other vehicles rather than static obstacles. Differently from previous GBSCMs, we characterize a real-world vehicular scenario by accurately modeling the path loss of the reflected paths via the radar cross-section (RCS) of the vehicles. Moreover, the V-CORE model provides adjustable parameters affecting traffic intensity, vehicle velocity, and road geometry. We then use the proposed model to compare the performance of OTFS to OFDM in different scenarios and get a deeper understanding of how the operational environment can impact the system behavior.

II. OTFS and OFDM System Model

Next, we briefly review the OFDM and OTFS modulations, specifically considering the cyclic prefix version for OFDM (CP-OFDM) and the Zero-Padding version for OTFS (ZP-OTFS). This ensures equal signal overhead between the two schemes, enabling a fair comparison.

A. Notation

Boldface characters denote vectors or matrices. $\mathbf{A}^{\mathsf{T}}$ and $\mathbf{A}^{\dagger}$ denote (resp.) the transpose and Hermitian transpose of a matrix. The (m,n)-th element of a matrix $\mathbf{A}$ is denoted by $\mathbf{A}(m,n)$. $\mathrm{vec}(\mathbf{A})$ is the column-wise vectorization of the matrix $\mathbf{A}$ and $\mathrm{vec}^{-1}_{M,N}(\mathbf{a})$ is the matrix formed by folding a vector $\mathbf{a}$ into an $M\times N$ matrix by filling it column wise. $\mathbf{F}_N$ is the normalized N-point discrete Fourier Transform (DFT) matrix, where the (i,k)-th element is $\mathbf{F}_N(i,k)=N^{-1/2}\mathrm{e}^{-\mathrm{j}2\pi ik/N}$. $\mathbb{E}\{\cdot\}$ denotes the expectation operator. Finally, $|\mathbf{a}_1-\mathbf{a}_2|$ denotes the Euclidean distance between vectors $\mathbf{a}_1$ and $\mathbf{a}_2$.

B. Discrete Time Baseband Channel

Following the notations in [9], [14], a summary of the model used to characterize the high mobility channel is given below. For each transmitted frame, we consider P propagation paths, where the path i, $i=1,\ldots,P$, has complex gain h_i, delay τ_i, and Doppler shift ν_i. The delay-Doppler channel response is:

$$h(\tau,\nu)=\sum_{i=1}^{P}h_i\delta(\tau-\tau_i)\delta(\nu-\nu_i) \tag{1}$$

and the corresponding continuous time-varying impulse response can be expressed as:

$$g(\tau,t)=\int_{-\infty}^{+\infty}h(\tau,\nu)\mathrm{e}^{j2\pi\nu(t-\tau)}d\nu\,. \tag{2}$$

Given a communication system with signal bandwidth B and frame duration T_{f}, the *normalized delays* and *normalized Doppler shifts* are defined as $\ell_i\triangleq\tau_i B$ and $\kappa_i\triangleq\nu_i T_{\mathrm{f}}$, respectively. The set of distinct normalized delays is defined as:

$$\mathcal{L}\triangleq\{\ell_i : i=1,\ldots,P\}\,. \tag{3}$$

The discrete-time model is obtained by sampling the waveform at intervals $t=qT_s$, where $0\leq q\leq N_s-1$, N_s being the number of samples per frame and T_s the sampling period. Assuming integer delay shifts (i.e., $\mathcal{L}\subset\mathbb{N}$) and defining $\ell_{\max}=\max(\mathcal{L})$, the discrete delay-time channel response can be expressed as the matrix $\mathbf{g}^{\mathrm{s}}\in\mathbb{C}^{(\ell_{\max}+1)\times N_s}$, with elements:

$$\mathbf{g}^{\mathrm{s}}(l,q)=\begin{cases}0 & \text{if } \mathcal{P}_l=\emptyset\\ \sum_{i\in\mathcal{P}_l}h_i\mathrm{e}^{\frac{\mathrm{j}2\pi}{N_s}\kappa_i(q-l)} & \text{otherwise}\end{cases} \tag{4}$$

where $\mathcal{P}_l$ is the set of paths with a common delay equal to l:

$$\mathcal{P}_l\triangleq\{i : i\in\{1,\ldots,P\}\wedge\ell_i=l\}\,. \tag{5}$$

The samples of the time-domain signal form the vector $\mathbf{s}\in\mathbb{C}^{N_s\times 1}$, which is transmitted through the high mobility channel. As a result, the received sampled signal is given by:

$$\mathbf{r}(q)=\sum_{l\in\mathcal{L}}\mathbf{g}^{\mathrm{s}}(l,q)\mathbf{s}(q-l)+\mathbf{w}(q) \tag{6}$$

for $q=0,\ldots,N_s-1$, where $\mathbf{w}\in\mathbb{C}^{N_s\times 1}$ represents the additive white Gaussian noise (AWGN) samples.

C. CP-OFDM

The OFDM grid is formed by M' subcarriers and N time slots. Information symbols are placed on the $M'\times N$ grid, resulting in the frequency-time domain signal $\mathbf{X}_{\mathrm{ft}}\in\mathbb{C}^{M'\times N}$. The time-domain vector, $\mathbf{s}'\in\mathbb{C}^{M'N\times 1}$, is obtained through a column-wise IDFT as:

$$\mathbf{s}'=\mathrm{vec}(\mathbf{F}^{\dagger}_{M'}\cdot\mathbf{X}_{\mathrm{ft}})=\left[\mathbf{s}'_0{}^{\mathsf{T}}\big|\cdots\big|\mathbf{s}'_{N-1}{}^{\mathsf{T}}\right]^{\mathsf{T}} \tag{7}$$

where $\mathbf{s}'_i\in\mathbb{C}^{M'\times 1}$. Finally, the cyclic prefix is inserted before every M' samples, forming the time-domain vector to be transmitted, $\mathbf{s}\in\mathbb{C}^{MN\times 1}$, given as:

$$\begin{aligned}\mathbf{s} &= \left[\quad \mathbf{s}_0{}^{\mathsf{T}} \quad\big|\cdots\big|\quad \mathbf{s}_{N-1}{}^{\mathsf{T}} \quad\right]^{\mathsf{T}}\\ &= \left[\mathbf{c}_0{}^{\mathsf{T}},\mathbf{s}'_0{}^{\mathsf{T}}\ \big|\cdots\big|\mathbf{c}_{N-1}{}^{\mathsf{T}},\mathbf{s}'_{N-1}{}^{\mathsf{T}}\right]^{\mathsf{T}}\end{aligned} \tag{8}$$

where $\mathbf{s}_i\in\mathbb{C}^{M\times 1}$ is the i-th block of the frame and the cyclic prefix $\mathbf{c}_i\in\mathbb{C}^{L_{\mathrm{CP}}\times 1}$ is given by:

$$\mathbf{c}_i=[\mathbf{s}'_i(M'-L_{\mathrm{CP}}),\mathbf{s}'_i(M'-L_{\mathrm{CP}}+1),\ldots,\mathbf{s}'_i(M'-1)]^{\mathsf{T}} \tag{9}$$

with $M=M'+L_{\mathrm{CP}}$, for $i=0,\ldots,N-1$.

Notice that the cyclic prefix length, L_{CP}, should be greater than or equal to the maximum delay shift, i.e., $L_{\mathrm{CP}}\geq\ell_{\max}$.

A total number of samples equal to $N_s{=}MN$ is required to transmit an OFDM frame. The overall frame duration is $T_{\text{f}}{=}NMT_s$, hence, assuming a sampling frequency equal to the Nyquist frequency (i.e., $f_s{=}B$), the signal bandwidth can be expressed as $B{=}M/T$, with $T{=}MT_s$ being the duration of each of the N blocks. The signal is received according to (6) and transformed back to the frequency-time domain through a column-wise DFT:

$$\mathbf{Y}_{\text{ft}} = \mathbf{F}_{M'} \cdot \text{vec}^{-1}_{M',N}(\mathbf{r}') \tag{10}$$

where $\mathbf{r}'{\in}\mathbb{C}^{M'N\times 1}$ represents the received samples after the cyclic prefixes have been removed. Finally, starting from $\mathbf{Y}_{\text{ft}}{\in}\mathbb{C}^{M'\times N}$, symbol detection is performed using minimum mean square error (MMSE) single-tap equalization, given its balanced trade-off between complexity and performance.

D. ZP-OTFS

In ZP-OTFS, symbols to be transmitted are placed on the $M{\times}N$ delay-Doppler grid, with M being the number of delay bins and N the number of Doppler bins, forming the delay-Doppler domain signal $\mathbf{X}_{\text{dd}}{\in}\mathbb{C}^{M\times N}$. The last L_{ZP} rows of $\mathbf{X}_{\text{dd}}$ consist of zero symbols. Analogously to CP-OFDM, the length of the zero padding L_{ZP} must satisfy $L_{\text{ZP}}{\geq}\ell_{\max}$. From the delay-Doppler domain, the transmitted time-domain vector, $\mathbf{s}{\in}\mathbb{C}^{MN\times 1}$, can be obtained using the Inverse Discrete Zak Transform (IDZT) [14]:

$$\mathbf{s} = \text{IDZT}\{\mathbf{X}_{\text{dd}}\} = \text{vec}(\mathbf{X}_{\text{dd}}\mathbf{F}_N^{\dagger}) \tag{11}$$

As discussed in the previous section, with $f_s{=}B$, we can express the signal bandwidth as $B{=}M/T$. Once $\mathbf{r}$ has been received according to (6), it is transformed into the delay-time domain as:

$$\mathbf{Y}_{\text{dt}} = \text{vec}^{-1}_{M,N}(\mathbf{r}) \in \mathbb{C}^{M\times N}\,. \tag{12}$$

The delay-time domain allows for the best trade-off between performance and complexity when adopting the maximum ratio combining (MRC) detection method, as detailed in [9].

III. Geometric Vehicular Channel Model

We now introduce our proposed V-CORE. In doing so, our main objective to define a model capable of generating realistic instances of the variables P, τ_i, ν_i, and h_i, $i{=}1,\ldots,P$, introduced in Sec. II-B. Notice that, unlike existing models such as EVA, the number of paths, P, is not a fixed parameter but can vary from frame to frame according to a distribution that depends on the traffic intensity and road geometry.

We consider a real-world vehicular scenario where a static Point of Access (PoA) transmits to an On-Board Unit (OBU) aboard a moving vehicle, and the PoA's signal is reflected by other vehicles along the road. The channel is formed by the direct signal path between PoA and OBU (line of sight (LoS) component), and the non-LoS (nLoS) components given by the one-hop reflections from other vehicles. Fig. 1 illustrates a nLoS path (green dashed line) generated by a reflecting vehicle.

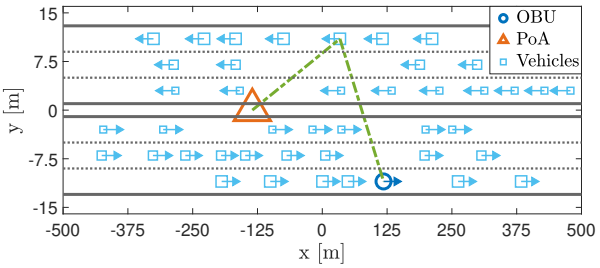

Fig. 1. Road scenario and example of a nLoS path (green dashed line) generated by a reflecting vehicle.

A. Road Scenario Generation

We specifically focus on a two-way road, with N_L lanes in each travel direction. For each transmitted frame, a different traffic scenario is generated, with each scenario being defined by the vehicles on the road, with their positions and velocities.

Specifically, vehicles enter lane $\ell{=}1,\ldots,N_L$ following a Poisson Point arrival process with arrival rate ρ_ℓ, where the index $\ell{=}1$ and $\ell{=}N_L$ indicate, respectively, the outermost (slow) lane and the innermost (fast) lane. A minimum inter-arrival time between adjacent vehicles is set to prevent vehicle collisions, ensuring that each previously generated vehicle has moved forward at least by its length. Each vehicle on lane ℓ travels at a random velocity v following a uniform distribution $U(v_\ell^{(\min)}, v_\ell^{(\max)})$, where $v_\ell^{(\min)}$ and $v_\ell^{(\max)}$ are the minimum and the maximum velocities on lane ℓ. The average vehicle velocity in lane ℓ is given by $\bar{v}_\ell{=}0.5{\cdot}(v_\ell^{(\min)}{+}v_\ell^{(\max)})$. Given the average distance between vehicles, μ_d, the Poisson arrival rate is derived as $\rho_\ell{=}\bar{v}_\ell/\mu_d$. If during the scenario generation, a vehicle approaches the one in front within the minimum safety distance, it will slow down to prevent rear-end accidents. Overall, this approach provides a realistic traffic scenario realization.

B. Channel Modeling

We recall that the PoA's signal is reflected by the other vehicles, which thus act as reflectors. For simplicity, let $i{=}1$ identify the LoS path, while $i{=}2,\ldots,P$ identify the nLoS paths. Regarding the LoS path, the channel gain is assumed to be circularly symmetric complex Gaussian distributed, i.e., $h_1{\sim}\mathcal{CN}(0,1)$. For a fair comparison, we set the same LoS distribution also for the EVA model. The LoS path on average has no attenuation: we are primarily concerned with the distribution of the reflected paths in different channel models, without making the LoS distribution relevant when we evaluate system performance.

Delay and Doppler shift of the LoS path are given by:

$$\tau_1 = \frac{d_1}{c}, \quad \nu_1 = \frac{1}{\lambda_c}\mathbf{v}_1^{\mathsf{T}}\frac{\mathbf{p}_{\text{A}} - \mathbf{p}_1}{d_1} \tag{13}$$

where $d_1{=}|\mathbf{p}_{\text{A}}{-}\mathbf{p}_1|$ is the PoA-OBU distance, with $\mathbf{p}_{\text{A}}$ and $\mathbf{p}_1$ being the position vectors of PoA and OBU, respectively. The velocity vector of the OBU is denoted with $\mathbf{v}_1$ and $\lambda_c{=}c/f_c$

is the signal wavelength, with f_c the signal carrier frequency and c the speed of light.

To determine the nLoS channel components, $i{=}2,\ldots,P$, we use a *bistatic radar* model where the PoA is the transmitter, the OBU the receiver, and the other reflecting vehicles the radar targets. The delay τ_i of a reflected path is given by:

$$\tau_i = \frac{d_i}{c} \tag{14}$$

where $d_i{=}|\mathbf{p}_\mathrm{A}{-}\mathbf{p}_i|{+}|\mathbf{p}_i{-}\mathbf{p}_1|{=}d_{\mathrm{A},i}{+}d_{i,1}$ is the total distance between PoA and OBU through the reflector, with $\mathbf{p}_i$ denoting the position vector of reflector i. In a bistatic radar system, the Doppler shift observed by the receiver depends on the velocity given by the sum of the velocity of the receiver relative to the target and the velocity of the target relative to the transmitter [15, Chap. 6], and can thus be expressed as:

$$\nu_i = \frac{1}{\lambda_c}\left[\mathbf{v}_i^\mathsf{T}\frac{\mathbf{p}_\mathrm{A}-\mathbf{p}_i}{|\mathbf{p}_\mathrm{A}-\mathbf{p}_i|} + (\mathbf{v}_1-\mathbf{v}_i)^\mathsf{T}\frac{\mathbf{p}_i-\mathbf{p}_1}{|\mathbf{p}_i-\mathbf{p}_1|}\right] \tag{15}$$

where $\mathbf{v}_i$ denotes the velocity vector of reflector i.

We adopt the *bistatic radar cross-section* of the target vehicle to determine the attenuation of the reflected path. The bistatic RCS quantifies the effective area in m^2 of a target that intercepts and reflects the incident signal energy from the transmitter toward the receiver. Given the i-th reflector, the bistatic RCS $\psi_i{=}f(\theta_i^{\mathrm{PoA}},\theta_i^{\mathrm{OBU}},f_c)$ depends on the object's shape, the signal frequency, f_c, and the angles of arrival θ_i^{PoA} and departure θ_i^{OBU} of the signal [16]. As a result, for nLoS paths, the complex gain can be derived as [17, Sec. 4-6]:

$$h_i = \frac{\lambda_c \mathrm{e}^{\mathrm{j}\phi_i}}{(4\pi)^2 d_{\mathrm{A},i} d_{i,1}}\sqrt{4\pi\psi_i G_\mathrm{A} G_\mathrm{O}} \tag{16}$$

where G_A and G_O are the antenna gains of the PoA and OBU and $\phi_i{\sim}U(0,2\pi)$ is the phase shift of the i-th path.
Additionally, we make the following assumptions:

1) PoA-OBU Distance: As mentioned in Sec. III, the number of paths P is not fixed. When the distance between the PoA and the OBU is large, the number of reflecting vehicles will increase on average, and so will the number of paths P. For each scenario generation, the OBU-PoA distance is uniformly drawn between a minimum and a maximum value, i.e., $d_1{\sim}U(d_{\min},d_{\max})$, and the transmit power P_{Tx} is adjusted to guarantee a 0 dB-path loss ($P_{\mathrm{Rx}}/P_{\mathrm{Tx}}$) at that distance, i.e.,

$$\frac{P_{\mathrm{Rx}}}{P_{\mathrm{Tx}}} = G_\mathrm{A}G_\mathrm{O}\left(\frac{\lambda_c}{4\pi d_1}\right)^2 = 1\ . \tag{17}$$

This approach allows the model to average the performance across multiple relative positions between the PoA and the OBU in a road environment, and to capture different numbers of reflectors and relative angles of the nLoS paths between PoA and OBU.

2) Energy of Reflected Paths: The proposed V-CORE generates multipath components with power at most 25 dB below the average LoS power $\mathbb{E}\{|h_1|^2\}$ (set at 0 dB), i.e.,

$$10\log_{10}\left(|h_i|^2\right) \geq -25 \text{ dB}, \quad \forall\ i=2,\ldots,P. \tag{18}$$

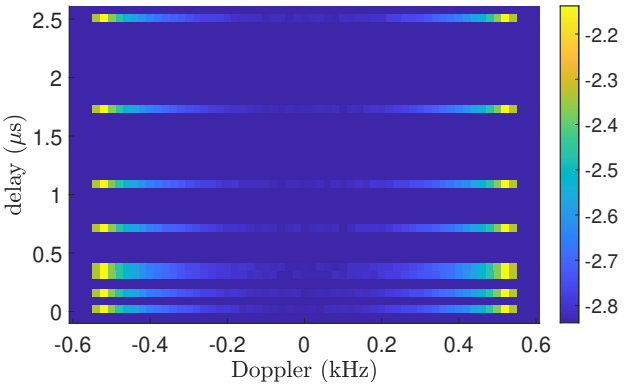

Fig. 2. EVA delay-Doppler bins probabilities in log-scale.

IV. Numerical Results

This section compares the frame error rates (FER) of OFDM and OTFS communication systems over (i) the V-CORE channel model described in Sec. III, and (ii) the commonly adopted EVA model. Before evaluating the performance of OFDM and OTFS, we provide an insight into the statistics of the reflected paths generated by EVA model and V-CORE in the delay-Doppler grid.

Concerning EVA, the first path is assumed to be the LoS path, while the remaining eight are the nLoS paths; also, each path gain is circularly symmetric complex Gaussian distributed and the Doppler shifts are Jakes distributed. The road parameters of V-CORE are displayed in Table I.

TABLE I
Default geometric channel parameters

PARAMETER	**VALUE**
Number of lanes, N_L	3
Minimum velocity in each lane, $v_\ell^{\min}$	{80, 100, 120} km/h
Maximum velocity in each lane, $v_\ell^{\max}$	{100, 120, 140} km/h
Vehicle length in each lane, L_ℓ	{16.0, 6.0, 4.4} m
Average distance between vehicles, μ_d	80 m
Safety distance between vehicles, D_s	20 m
Lane width, W	4 m
Space between travel directions, D_t	2 m
Minimum PoA-OBU distance, $d_{\min}$	50 m
Maximum PoA-OBU distance, $d_{\max}$	700 m

For EVA, the sole parameter is the maximum vehicle speed, which is set to 160 km/h. A generic nLoS path is characterized by a specific delay-Doppler value, whose joint probability has been estimated.

Figures 2 and 3 illustrate the results for EVA and V-CORE, respectively. The color of each point represents the discrete probability (on a logarithmic scale) that an nLoS path falls within the indicated delay-Doppler bin. The probability of each bin has been empirically estimated across nLoS paths over multiple scenario realizations.

In Fig. 2 (referring to EVA model), along the delay axis, the 8 reflected paths are clearly visible and well separated. Along the Doppler axis, the Jakes distribution is recognizable, with peak values at the edges. In Fig. 3 (referring to V-CORE), along the delay axis, one can still note some separated rows,

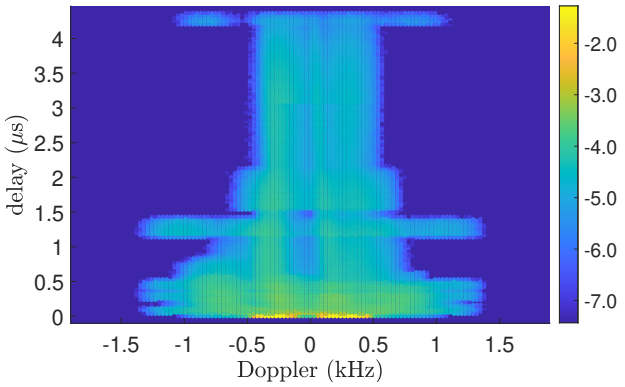

Fig. 3. V-CORE delay-Doppler bins probabilities in log-scale.

but they are less distinct compared to those of EVA. Along the Doppler axis, the Doppler shifts do not follow the Jakes distribution as in the EVA model, since the reflectors are not evenly distributed around the receiver. In fact, in a highway scenario, the velocity vector of the PoA-OBU-reflector system is mainly aligned along the road, rather than being distributed across all angles as in a urban environment.

The maximum Doppler shift in V-CORE is given by $\nu_{\max}{=}3v_{N_L}^{(\max)}/\lambda_c$, corresponding to the case where the OBU and the reflector are approaching each other at the maximum velocity, while the OBU is also approaching the PoA. An analogous argument applies to the minimum Doppler shift, $\nu_{\min}{=}{-}3v_{N_L}^{(\max)}/\lambda_c$, where the OBU is moving away from both the PoA and the reflector. We then simulated OFDM and OTFS systems to compare their FER performance, under our V-CORE and the standard EVA model. The key assumptions we made are listed below, while the OFDM/OTFS parameter settings can be found in Table II.

1) Detection: As motivated in Sec. II, we adopt MMSE single-tap equalization for OFDM and delay-time MRC detection for OTFS.

2) Channel Estimation: Channel state information (CSI) is assumed to be known at the receiver side. Therefore, the receiver knows the noise variance σ^2, the complex gains h_i, the normalized delays ℓ_i, and the Doppler shifts κ_i of each path i. In practice, the receiver cannot distinguish different physical paths falling in the same delay-Doppler bin. Hence, two physical paths i and j, with $\ell_i{=}\ell_j$ and $[\kappa_i]{=}[\kappa_j]$, can be merged into a single path k with complex gain $h_k{=}h_i{+}h_j$. Without loss of generality, we order the remaining paths from $i{=}1$ to P^*, where $P^*{<}P$ denotes the number of distinct resolved paths.

3) Signal-to-noise Ratio (SNR): We define the expected SNR as:

$$\overline{\text{SNR}} \triangleq \frac{E_s}{\sigma^2}\mathbb{E}\{\|\boldsymbol{h}\|^2\} \tag{19}$$

where $\|\boldsymbol{h}\|^2{=}\sum_{i=1}^{P^*}|h_i|^2$ and E_s is the average energy per symbol. Note that, since we are considering channel models affected by fading events, the instantaneous SNR is not fixed but varies from frame to frame. The definition of the average SNR in (19) is consistent with the SNR of a point-to-point multiple-input single-output (MISO) channel when a maximum-ratio transmission (MRT) precoding vector is adopted [18, Chap. 3]. In fact, MRC in OTFS achieves an analogous effect by coherently combining the different multipath components.

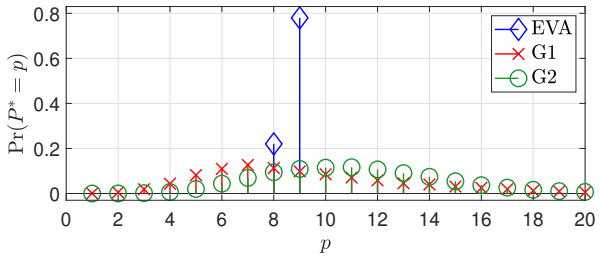

Fig. 4. Probability mass function of P^* for the V-CORE (under the road scenarios G1 and G2) and the EVA model.

4) Geometric Coherence Time: We assume that the channel remains constant during the transmission of an entire frame. For instance, if $M{=}512$ and $\Delta f \triangleq 1/T{=}30$ kHz, the system has a spatial resolution equal to $c{\cdot}T_s{=}c/M\Delta f{\approx}20$ m, where c is the speed of light. If $N{=}128$, the frame duration is $T_{\text{f}}{=}N/\Delta f{=}4.3$ ms. This implies that a vehicle traveling at 160 km/h would move less than 0.2 m in this interval, i.e., less than the spatial resolution, which allows us to assume that the channel remains constant over the frame duration.

TABLE II
SYSTEM PARAMETERS

PARAMETER	VALUE
Bandwidth, B	15.36 MHz
Delay bins (subcarriers), M	512
Doppler bins (time slots), N	128
Subcarrier spacing, Δf	30 kHz
Frame duration, $T_{\text{f}}{=}N/\Delta f$	4.2 ms
Carrier frequency, f_c	3.6 GHz
Data modulation	4-QAM

We evaluate the V-CORE in two different highway geometry scenarios, referred to as G1 and G2, characterized by the parameters presented in Table III. The missing geometric parameters are set as displayed in Table I.

TABLE III
ROAD SCENARIO PARAMETERS FOR V-CORE

	PARAMETER	VALUE
G1	$v_\ell^{\max}$	{110, 130, 150} km/h
G2	Number of lanes N_L	5
	$v_\ell^{\min}$	{70, 85, 100, 115, 130} km/h
	$v_\ell^{\max}$	{100, 115, 130, 145, 160} km/h
	Veh. length in each lane L_ℓ	{16.0, 6.0, 6.0, 6.0, 4.4} m
	Ave. dist. between veh. μ_d	40 m
	Safety dist. between veh. D_s	15 m

Figures 4 and 5 show, respectively, the probability mass function of P^* and the OFDM/OTFS performance for the V-CORE model under the two different road scenarios, G1 and G2, and for the EVA model. In particular, Fig. 4 underscores that the 9 paths in EVA are well distinguishable due to their

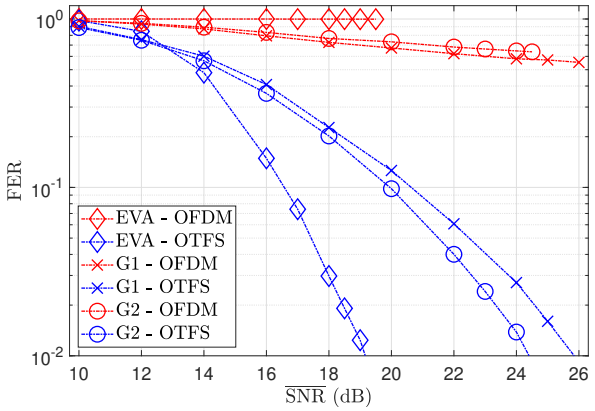

Fig. 5. FER vs. $\overline{\text{SNR}}$: OFDM and OTFS comparison under the V-CORE in road scenarios G1 and G2 and the EVA model.

distinct delays and Doppler shifts, allowing OTFS to perform optimally. In contrast, under the V-CORE model, the number of paths spans from 1 to 20, with a larger number of paths being more likely to occur in G2 due to the higher number of lanes and reflective vehicles. Relative to the EVA model, the variable number of paths per channel realization in the V-CORE model results in degraded average performance. Fig. 5 shows that OTFS outperforms OFDM in all high-mobility traffic models and scenarios. Further, the results confirm the above observations, highlighting that OTFS under the EVA model outperforms OTFS under V-CORE, with, e.g., a remarkable gain of over 5 dB at FER=10^{-2}. This is because, although we set the EVA's maximum speed parameter to 160 km/h, nLoS paths in EVA are stronger than under V-CORE, as the former is specifically designed to capture signal propagation in urban and suburban areas. Moreover, the significant difference in delays between the paths is rather optimistic, thus further contributing to an overestimate of the performance. In contrast, in the V-CORE G1 and G2 scenarios, the reflectors are aligned along the horizontal dimension of the road, thus significantly reducing delay and Doppler shift diversity among the different paths. It follows that V-CORE provides more realistic results for high-speed scenarios. As further evidence, OTFS performs better in G2 than in G1 because G2 features two additional lanes, which increases diversity by including more vehicles along the vertical dimension of the road. In contrast, OFDM exhibits an opposite trend compared to OTFS when evaluated through the different channel models, as it struggles to deal with more paths.

V. Conclusions

We developed and analyzed a new realistic channel model to evaluate OTFS and OFDM performance in high-speed vehicular scenarios. The proposed Geometric-based Stochastic Channel Model includes features such as reflected path modeling, radar cross-section of reflectors, and tunable traffic intensity and road geometry. Our model thus provides a more comprehensive understanding of OTFS performance in high-speed vehicular scenarios compared to state-of-the-art models like the EVA one, which is limited to low-speed urban and suburban areas. Key findings highlight the significant impact of traffic conditions on OTFS and OFDM performance. Nonetheless, even with our new, accurate channel model, OTFS consistently shows clear advantages over OFDM, achieving a gain of several dB, by effectively exploiting channel diversity and coherently combining the paths of multiple reflecting vehicles.

Acknowledgments

This work was supported by the EC through Grant No. 101096379 (CENTRIC project). The work of E. Viterbo was supported by the Australian Research Council (ARC) through the Discovery project: DP200100096.

References

[1] T. Wang, J. Proakis, E. Masry, and J. Zeidler, "Performance Degradation of OFDM Systems due to Doppler Spreading," *IEEE Transactions on Wireless Communications*, vol. 5, no. 6, pp. 1422–1432, 2006.

[2] R. Hadani, S. Rakib, M. Tsatsanis, A. Monk, A. J. Goldsmith, A. F. Molisch, and R. Calderbank, "Orthogonal Time Frequency Space Modulation," in *IEEE WCNC*, 2017, pp. 1–6.

[3] 3GPP, "Evolved Universal Terrestrial Radio Access (E-UTRA); User Equipment (UE) Radio Transmission and Reception," Technical Specification Group Radio Access Network, Tech. Rep. TS 36.101.

[4] ITU, "Rec. ITU-R m.1034-1: Requirements for the radio interface(s) for international mobile telecommunications-2000," 1997.

[5] K. Schaubach, N. Davis, and T. Rappaport, "A Ray Tracing Method for Predicting Path Loss and Delay Spread in Microcellular Environments," in *IEEE VTS*, 1992, pp. 932–935 vol.2.

[6] P. Petrus, J. Reed, and T. Rappaport, "Geometrical-Based Statistical Macrocell Channel Model for Mobile Environments," *IEEE Transactions on Communications*, vol. 50, no. 3, pp. 495–502, 2002.

[7] J. Karedal, F. Tufvesson, N. Czink, A. Paier, C. Dumard, T. Zemen, C. F. Mecklenbrauker, and A. F. Molisch, "A Geometry-Based Stochastic MIMO Model for Vehicle-to-Vehicle Communications," *IEEE Transactions on Wireless Communications*, vol. 8, no. 7, pp. 3646–3657, 2009.

[8] R. T. Rakesh and E. Viterbo, "Geometry Based Stochastic Channel Modeling using Ambit Processes," in *IEEE WCNC*, 2020, pp. 1–6.

[9] T. Thaj and E. Viterbo, "Low Complexity Iterative Rake Decision Feedback Equalizer for Zero-Padded OTFS Systems," *IEEE Transactions on Vehicular Technology*, vol. 69, no. 12, pp. 15 606–15 622, 2020.

[10] K. R. Murali and A. Chockalingam, "On OTFS Modulation for High-Doppler Fading Channels," in *ITA*, 2018, pp. 1–10.

[11] H. Zhang, X. Huang, and J. A. Zhang, "Comparison of OTFS Diversity Performance over Slow and Fast Fading Channels," in *IEEE/CIC ICCC*, 2019, pp. 828–833.

[12] F. Wiffen, L. Sayer, M. Z. Bocus, A. Doufexi, and A. Nix, "Comparison of OTFS and OFDM in Ray Launched sub-6 GHz and mmWave Line-of-Sight Mobility Channels," in *IEEE PIMRC*, 2018, pp. 73–79.

[13] T. Blazek, H. Groll, S. Pratschner, and E. Zochmann, "Vehicular Channel Characterization in Orthogonal Time-Frequency Space," in *IEEE ICC Workshops*, 2019, pp. 1–5.

[14] Y. Hong, T. Thaj, and E. Viterbo, *Delay-Doppler Communications Principles and Applications*. AP-Elsevier, London, UK, Feb. 2022.

[15] N. J. Willis, *Bistatic Radar*, ser. Radar, Sonar and Navigation. Institution of Engineering and Technology, 2004. [Online]. Available: https://digital-library.theiet.org/content/books/ra/sbra003e

[16] S. Rao, D. Wilton, and A. Glisson, "Electromagnetic Scattering by Surfaces of Arbitrary Shape," *IEEE Transactions on Antennas and Propagation*, vol. 30, no. 3, pp. 409–418, 1982.

[17] Naval Air Warfare Center Weapons Div Point Mugu, CA, Avionics Department Code, 450000E, *Electronic Warfare and Radar Systems Engineering Handbook*, 4th ed., Sep. 2013.

[18] E. Björnson and Özlem Tuğfe Demir, *Introduction to Multiple Antenna Communications and Reconfigurable Surfaces*. Boston-Delft: Now Publishers, 2024. [Online]. Available: http://dx.doi.org/10.1561/9781638283157